Check for updates

Neha Vishnoi[1]
Department of Mechanical Engineering,
Indian Institute of Technology Ropar,
Rupnagar 140001, Punjab, India
e-mail: 2018mez0019@iitrpr.ac.in

Vikrant Gupta
Department of Mechanics and
Aerospace Engineering,
Southern University of Science and Technology,
Shenzhen, Guangdong Province 518055, China,
e-mail: vikrant@sustech.edu.cn

Aditya Saurabh
Department of Mechanical Engineering,
Indian Institute of Technology Kanpur,
Kanpur 208016, Uttar Pradesh, India
e-mail: asaurabh@iitk.ac.in

Lipika Kabiraj[1]
Department of Mechanical Engineering,
Indian Institute of Technology Ropar,
Rupnagar 140001, Punjab, India
e-mail: lipika.kabiraj@iitrpr.ac.in

System Parameter Identification of a Colored-Noise-Driven Rijke Tube Simulator

In this paper, we report an experimental investigation on the influence of colored noise (generated by the Ornstein–Uhlenbeck (OU) process) on thermoacoustic coupling in an electro-acoustic Rijke tube simulator. In the absence of noise, the simulator exhibits subcritical Hopf bifurcation. Although noise in a practical system has a finite correlation time, yet the system identification methods are based on the assumption of white noise. In this study, we investigate the effects of correlation time, and intensity of colored noise on the estimation of the growth rates of acoustic oscillations determined using Fokker–Planck equation in stable, bistable, and linearly unstable regions. Subsequently, we compare the findings against results obtained considering white noise approximations. We report the observed deviation of the estimated growth rates from the actual values as a function of noise intensity and correlation time. We find that with the colored noise model, the deviation in the estimated growth rates lies within the range of 0–10% compared to the deviation of 5–25% observed considering the white noise approximation. We also report that increasing noise amplitudes leads up to a deviation of approximately 30% in the estimated growth rates from the actual values. [DOI: 10.1115/1.4055212]

Downloaded from http://asmedigitalcollection.asme.org/gasturbinespower/article-pdf/144/9/091017/6912725/gtp_144_09_091017.pdf by Indian Institute of Technology-Ropar user on 27 September 2022

1 Introduction

Thermoacoustic instability is a major technical problem in gas turbine combustors. The instability is characterized by self-excited large-amplitude pressure oscillations that develop spontaneously as a result of constructive feedback between heat release fluctuations and acoustics of the combustor [1]. The oscillations result in premature wear of combustor components and may even lead to catastrophic failures. Suppressing/eliminating these instabilities is presently a subject of intense research. The aspect of thermoacoustic instability we are investigating is the effect of noise on the feedback coupling responsible for thermoacoustic oscillations. An effective method of controlling the instabilities is to implement acoustic dampers such as the Helmholtz resonator [2] in practical combustors to absorb the energy of the combustor acoustic modes. Accurate estimates of stability margins and linear growth rates of self-sustained oscillations are important for designing the damping devices [3].

It is known that as combustor operating conditions (temperature, fuel flowrate, total flowrate, etc.) are varied, the onset of thermoacoustic instability occurs via a Hopf bifurcation. There are two variants of Hopf bifurcation, supercritical and subcritical; both of which are observed in thermoacoustic systems [4,5]. The characteristic feature of Hopf bifurcations is that the system develops oscillations (often single frequency limit cycle oscillations, but more complex states with multiple frequencies are also possible [6,7]) at a critical parameter value known technically as the Hopf point. The distinguishing feature of subcritical Hopf bifurcation, which is more common than supercritical bifurcation in combustors, is the presence of a bistable region in the parameter space prior to the Hopf point. In the bistable regime, the system can either be stable (no oscillations) or unstable (oscillations). Instability may be triggered within the bistable regime via external or inherent noise [4,5,8].

Gas turbine combustors are inherently noisy environments. Noise is either generated directly by unsteady combustion or indirectly by turbulence or flow separation. Several investigations have investigated the effect of noise on triggering [9,10], stability margins [11,12], and extracting the growth/decay rate of the instability in the various regimes of the Hopf bifurcation from noisy combustor data [13–18]. The authors [13–18] proposed several system identification methods using the amplitude and phase stochastic differential equations (SDEs) for Van der Pol oscillators. Later, Boujo and Noiray [15] reported improvements in the accuracy of the Fokker–Planck method of system identification by incorporating adjoint-based optimization. Recently, Vishnoi et al. [19] investigated the effect of varying white noise amplitudes on system identification parameters in a prototypical thermoacoustic system. The authors extracted the growth rates from noisy pressure time-series by making use of the theoretical methods proposed by Noiray and Schuermans [13] and reported that noise intensity over and underestimate the growth rates in the stable and linearly unstable regions, respectively.

Recent investigation of the effect of noise on system dynamics prior to the bifurcation has led to important results that could potentially lead to predictive tools. Kabiraj et al. [20] experimentally investigated the response of a prototypical thermoacoustic system to varying amplitudes of acoustic white noise signals for a range of operating conditions in the subthreshold region. The experimental results reported identify the presence of coherence resonance: an interaction between noise and the system such that coherent oscillations are induced when the system is stable. The investigation was further expanded in Saurabh et al. [21] to show the presence of stochastic "P-bifurcations": qualitative changes in the statistical characteristics of pressure fluctuations as the noise intensity is increased. Lee et al. [22] proposed an input–output framework where an extrinsic noise source helps predict the bifurcation properties and limit cycle amplitudes using the linearly stable data before Hopf point. The authors reported that prebifurcation data of a noisy system could accurately predict the Hopf bifurcation properties, such as its location and super/subcritical nature.

Most often, the reported works on noise-induced dynamics have adopted white Gaussian noise to model stochastic source of noise. However, experiments have shown that noise in combustors, in particular from the turbulent flame, is predominantly of a

[1]Corresponding authors.

Manuscript received June 29, 2022; final manuscript received July 23, 2022; published online August 26, 2022. Editor: Jerzy T. Sawicki.

Copyright © 2022 by ASME

low-pass character [23–25]. Noise in combustors is better represented by colored noise with a power density that decreases with the increasing frequency. Previous studies have shown that the correlation time of colored noise significantly affects the statistical response of a system. In the thermoacoustic community, Waugh and Juniper [9] investigated the effect of three different types of noise on triggering phenomenon in the bistable regime: pink noise (low-pass in character), white noise, and blue noise. In the study, noise was applied in the system in two ways: short bursts and continuously. The authors observed that among the three types, pink noise is more effective in causing triggering than white and blue noise. Li et al. [26] numerically investigated the effects of Ornstein–Uhlenbeck (OU) type colored noise-induced dynamics on the stochastic properties of thermoacoustic oscillations in the vicinity of supercritical Hopf bifurcation point. The authors reported that correlation time and noise intensity have significant but opposite effects on the properties of noise-induced oscillations. Bonciolini et al. [24,25] studied the comparative dynamical and statistical response of a supercritical thermoacoustic system when driven by both white and colored noise. The white noise approximation, generally employed for data analysis and system identification, was compared with Ornstein–Uhlenbeck noise model, and the effect of variation of correlation time and noise power was investigated. Significant differences in the amplitude probability density function were observed for higher noise intensities and longer correlation times in comparison to white noise. The authors also reported the importance of preprocessing of the pressure-time data for robust system identification. Thus, it becomes important to use accurate noise models for system identification of gas turbine systems.

In this work, we report an experimental investigation on the influence of Ornstein–Uhlenbeck type colored noise on thermoacoustic coupling using an electro-acoustic Rijke tube simulator—a prototypical thermoacoustic system—which exhibits instabilities via subcritical Hopf bifurcation. The simulator is represented in Fig. 1 and is described in Sec. 2.2 in detail. Specifically, the objective is to investigate the effects of noise color and intensity on growth rates estimation and to show the limitation of white noise approximation in the stable, bistable, and linearly unstable regions so that a better understanding of the colored noise driven thermoacoustic system can be obtained.

The sections that follow are divided into four main sections: first, we introduce the theoretical background, and details of the experiments. Subsequently, we discuss the effects of noise correlation time and its intensity on probability distribution function and further the estimation of growth rates. Finally, we state the main conclusions and implications of the findings of our study.

2 Electro-Acoustic Rijke Tube System

2.1 Rijke Tube: Background. Rijke tube [27–29] is a simple thermoacoustic system consisting of a hot wire gauze placed inside a tube with open ends. Thermoacoustic instability arises in this system due to feedback coupling between acoustic oscillations associated with duct acoustic modes and heat release rate fluctuations from the hot wire gauze. A theoretical model for thermoacoustic instability in the Rijke tube [30] is developed by linearizing the momentum and energy equations of the acoustic field, assuming that the effects of mean flow and temperature gradient are negligible. Only planar, longitudinal acoustic modes are considered. The corresponding dimensionless forms of the acoustic momentum and energy equations for the Rijke tube are given as

$$\begin{aligned}\frac{\partial u}{\partial t} &= -\frac{1}{\gamma M_a}\frac{\partial p}{\partial x}\\ \frac{\partial p}{\partial t} &= -\gamma M_a \frac{\partial u}{\partial x} - \zeta p + \dot{Q}'\delta(x - x_{\text{fn}})\end{aligned} \tag{1}$$

For nondimensionalization, the duct longitudinal coordinate is normalized by the length of the duct, L_a to give x; time, by L_a/c_0 (c_0 is the speed of sound) to give t; velocity fluctuations are normalized by u_0 to give u; and acoustic pressure is normalized by mean pressure p_0 to give p. $\dot{Q}'$ represents the dimensionless heat release rate fluctuations, normalized by $\frac{\rho c_0^3}{\gamma(\gamma-1)}$, where γ is the ratio of specific heat at constant pressure and volume ($\gamma = c_p/c_v$). ζ represents the acoustic damping in the system. M_a is the Mach number (u_0/c_0) of the mean flow, and δ is the standard Dirac distribution employed to indicate that the heat release occurs at $x_{\text{fn}} = x_f/L_a$, where x_f is the heater location. A model for the heat release rate fluctuations, $\dot{Q}'$ is required, and the same is taken as a modified form of King's law, as in Heckl [28]

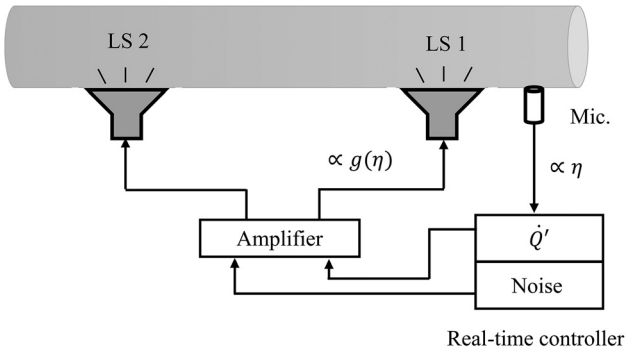

Fig. 1 Schematic diagram of the electro-acoustic Rijke tube simulator. It is a cylindrical duct closed at both the ends and is fitted with acoustic driver units and a microphone. A feedback loop inducing electro-acoustic oscillations is generated by routing microphone to LS 1 via RTC. Noise is fed through LS 2.

$$\dot{Q}' = K\left[\sqrt{\left|\frac{1}{3} + u_f(t-\tau)\right|} - \frac{1}{\sqrt{3}}\right] \tag{2}$$

where τ is the time-delay representing thermal inertia of heat transfer from the hot wire gauze [31], normalized by L_a/c_0; K is the normalized heater power, which is a function of physical and thermodynamic properties of the hot wire gauze and the fluid. u_f is the nondimensional acoustic velocity at x_{fn}.

Acoustic velocity, u, and pressure, p are projected onto the first N Galerkin base modes resulting in a set of $2N$ ordinary differential equations. The Galerkin modes satisfy the closed–closed boundary condition simulated by the electro-acoustic Rijke tube

$$\begin{aligned}p(x,t) &= \sum_{j=1}^{N}\frac{\dot{\eta}_j(t)}{j\pi}\gamma M_a \cos(j\pi x)\\ u(x,t) &= \sum_{j=1}^{N}\eta_j(t)\sin(j\pi x)\end{aligned} \tag{3}$$

On substituting this decomposition in acoustic momentum and energy equations (Eq. (1)) and adding additive noise, we obtain

$$\begin{aligned}&\frac{d\eta_j}{dt} = \dot{\eta}_j\\ &\frac{d\dot{\eta}_j}{dt} + \zeta_j\dot{\eta}_j + (j\pi)^2\eta_j\\ &\quad = Kj\pi\left[\sqrt{\left|\frac{1}{3} + u_f(t-\tau)\right|} - \sqrt{\frac{1}{3}}\right] \times \cos(j\pi x_f) + \xi_j\end{aligned} \tag{4}$$

The damping term ζ_j is modeled as $\zeta_j = C_1 j + C_2\sqrt{1/j}$, with C_1 and C_2 in accordance with Matveev and Culick [32] and Sterling and Zukoski [33].

Downloaded from http://asmedigitalcollection.asme.org/gasturbinespower/article-pdf/144/9/091017/6912725/gtp_144_09_091017.pdf by Indian Institute of Technology-Ropar user on 27 September 2022

Additive noise, ξ_j in Eq. (4), is modeled by a Gaussian white noise and the Ornstein–Uhlenbeck process in two different set of experiments. The latter has previously been employed for modeling systems where external noise is expected to have a low-pass nature [25,34]. In combustors as well, noise has a low pass character. In particular, acoustic noise from the turbulent flame is known to be characterized by a cutoff frequency beyond which power density decays as a power law: $P \propto f^{-r}$, where $2 < r < 3.4$ [23].

ξ_j when modeled as an OU process satisfies the following Langevin equation [25,26]:

$$\dot{\xi}(t) = -\frac{1}{\tau_c}\xi(t) + \frac{\sqrt{D}}{\tau_c}\epsilon(t) \tag{5}$$

where τ_c denotes the autocorrelation time of noise and correspondingly controls the cutoff frequency in the power spectrum. D denotes the noise intensity and $\epsilon(t)$ is a Gaussian white noise of intensity, Γ, with zero mean and unit variance. Thus, white noise is a limiting case of the OU noise, as $\tau_c \to 0$: the shorter τ_c, the closer ξ is to white noise [35]. This is illustrated in Fig. 2 along with the oscillator's response to the input OU noise. The OU noise has the following statistical properties:

$$\langle \xi(t) \rangle = 0; \quad \langle \xi(t)\xi(t') \rangle = s^2 \exp\left(-\frac{|t-t'|}{\tau_c}\right)$$

where the parameter, $s^2 = D/\tau_c$, is the variance of the OU process given by its second moment, $\langle \xi^2 \rangle$. The power spectrum of $\xi(t)$ is given as

$$S_{\xi\xi}(\omega) = \frac{\Gamma}{2\pi}\frac{D}{1+\omega^2\tau_c^2}$$

In the limit $\tau_c \to 0$ and $D \to 1$, we get $S_{\xi\xi}(\omega) \to \Gamma/2\pi = S_{\epsilon\epsilon}(\omega)$ [35].

Two different interpretations of OU noise can be considered for investigating the effect of correlation time (color) and noise power variation on a system: (i) by keeping variance, s^2, constant and varying τ_c [36]. In this case, the total power of the noise (the area under the power spectral density of the process) is conserved on varying the correlation time; (ii) by keeping the powers provided by ξ and by a white noise of intensity Γ in a band around the system's natural frequency equal, i.e., $\int_{\omega_1}^{\omega_2} S_{\xi\xi} d\omega = \int_{\omega_1}^{\omega_2} \Gamma/2\pi d\omega$ [25]. In this case, the intensity of ξ is adjusted by the coefficient D, evaluated using the following expression:

$$D = \frac{\tau_c(\omega_2 - \omega_1)}{atan(\omega_2\tau_c) - atan(\omega_1\tau_c)}$$

The latter method makes an assumption that the noise at and around the peak frequency is important for system behavior. Whereas, the first interpretation is more closer to the practical case as noise power is not fixed within a band. In this work, we study the effects of correlation time and noise power variation on the response of a prototypical thermoacoustic system using both the above interpretations for generating OU noise. These interpretations of the OU noise are considered to be the driving force for the Rijke tube model given by Eq. (4).

It is convenient to recast the Rijke tube model using the amplitude-phase coordinates. This substitution is reasonable as, in practical cases, the thermoacoustic systems are categorized as "weakly" amplified/damped systems [24]. For the jth mode, substituting $\eta_j(t) \approx a_j(t)\cos[\omega_j t + \varphi_j(t)] = a_j(t)\cos\phi_j(t)$ and the model (Eq. (5)) for ξ in Eq. (4) followed by stochastic averaging [37], we get the following SDEs:

$$\begin{aligned}
\dot{a}_j &= -\frac{\zeta_j a_j}{2} + \frac{c_1\tau a_j}{2} + \frac{3c_3\tau^3 a_j^3\omega_j^2}{8} + \frac{3c_3\tau a_j^3}{8} + Q_a(a,\phi) + \frac{\xi_j}{\omega_j}(\sin\phi) \\
\dot{\varphi}_j &= \frac{c_1}{2\omega_j} + \frac{3c_3 a_j^2}{8\omega_j} + \frac{3c_3\tau^2 a_j^2\omega_j}{8} + Q_\phi(a,\phi) + \frac{\xi_j}{a_j\omega_j}(\cos\phi)
\end{aligned} \tag{6}$$

where $Q_a(a,\phi)$ and $Q_\phi(a,\phi)$ are the sum of first-order sine and cosine terms that become zero after time-averaging and

$$c_1 = \frac{\sqrt{3}Kj\pi}{4}\sin(2j\pi x_f); \quad c_2 = -\frac{3\sqrt{3}Kj\pi}{16}\sin(2j\pi x_f)\sin(j\pi x_f);$$
$$c_3 = \frac{9\sqrt{3}Kj\pi}{32}\sin(2j\pi x_f)\sin^2(j\pi x_f)$$

Considering the Fokker–Planck equation [38] associated with Eq. (6), we can derive the stationary probability distribution (PDF) for the amplitude of the OU noise driven Rijke tube simulator as

$$P_c(a_j) = C_c a_j \exp\left[\left(-\zeta_j + c_1\tau\right)\frac{4\omega_j^2 a_j^2}{\Gamma}\frac{\left(1+\omega_j^2\tau_c^2\right)}{\sqrt{D}} + \left(1+\omega_j^2\tau^2\right)\frac{12c_3\tau a_j^4\omega_j^2}{8\Gamma}\frac{\left(1+\omega_j^2\tau_c^2\right)}{\sqrt{D}}\right] \tag{7}$$

and for the white noise driven Rijke tube simulator as

$$P_w(a_j) = C_w a_j \exp\left[\left(-\zeta_j + c_1\tau\right)\frac{4\omega_j^2 a_j^2}{\Gamma} + \left(1+\omega_j^2\tau^2\right)\frac{12c_3\tau a_j^4\omega_j^2}{8\Gamma}\right] \tag{8}$$

where C_c and C_w are the normalization constants such that $\int_0^\infty P(a_j)da_j = 1$. The detailed derivations for Eqs. (6)–(8) are given in Appendix.

For a given set of parameters $(\zeta_j, \tau, \omega_j, c_1, c_3)$, $P_w(a_j)$ is dependent only on white noise intensity, Γ, whereas, $P_c(a_j)$ is also dependent on τ_c and D. Equations (7) and (8) differ in normalization constants and a factor $\frac{(1+\omega_j^2\tau_c^2)}{\sqrt{D}}$ in the exponent. For $\tau_c \to 0$ and $D \to 1$ [35], this factor is close to 1, resulting in Eqs. (7) and (8) to be identical. The significant difference in the two expressions for P_w and P_c occurs for larger values of τ_c that is investigated in detail in this study. This Fokker–Planck formulation is used for system identification later in the study following the methods 3 and 4 proposed by Noiray and Schuermans [13].

2.2 Rijke Tube Simulator. To investigate thermoacoustic instability in a controlled setting, we take inspiration from Noiray

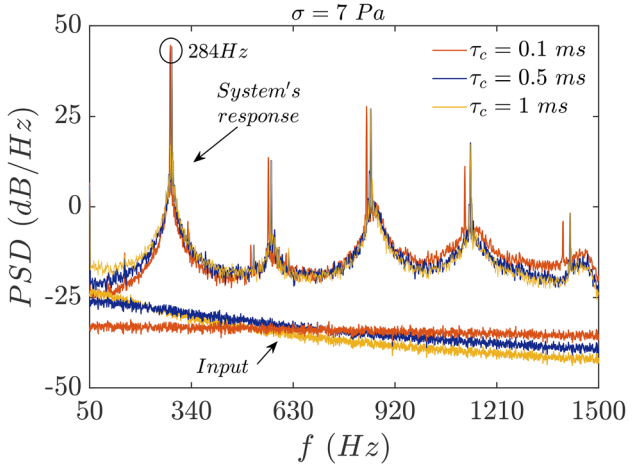

Fig. 2 Power spectrum of the input, $\xi(t)$, and the corresponding oscillator response for three different values of correlation time, τ_c. The shorter the τ_c, the closer ξ is to white noise (a flat power spectrum).

Downloaded from http://asmedigitalcollection.asme.org/gasturbinespower/article-pdf/144/9/091017/6912725/gtp_144_09_091017.pdf by Indian Institute of Technology-Ropar user on 27 September 2022

and Schuermans [13] and conduct experiments with noise in an electro-acoustic Rijke tube simulator designed to mimic the classical Rijke tube. The investigated setup (Fig. 1) consists of a cylindrical duct closed at both ends and fitted with two acoustic driver units, a condenser microphone combined with a signal conditioner, and a real-time controller (RTC). An electro-acoustic feedback loop is generated in this simulator by routing the microphone to loudspeaker 1 (LS 1) through a RTC. The Rijke tube model (Eq. (4)) is simulated in the RTC. Simultaneously, loudspeaker 2 (LS 2) is fed by noise modeled as white noise in one set of experiments and an OU process in a separate set. We consider K as the control parameter for the simulator while choosing the values of the other Rijke tube parameters as: $\tau = 0.2, C_1 = 0.1, C_2 = 0.06$, and $x_f = 0.25$ [31]. Some of the experiments were repeated multiple times to check for repeatability. Prior to experiments with the Rijke tube simulator and noise, the cold decay rate (with $K = 0$) of Rijke tube simulator was checked; in all tests, the exponential decay rate was consistently obtained with a value $v = 11 \pm 1 s^{-1}$.

2.3 Subcritical Hopf Bifurcation. For the noise-free system, as the parameter K is gradually increased from 0, thermoacoustic instability spontaneously appears in the initially stable system; a stable limit cycle is observed. The bifurcation plot, pressure-time traces, and corresponding power spectrum are presented in Fig. 3. It is observed that the simulator evolves through a subcritical Hopf bifurcation characterized by a Hopf point and saddle (also fold) point at $K_H = 0.64$ and $K_{SN} = 0.44$, respectively. The bistable region exists for $0.44 < K < 0.64$. The region before the fold point ($K < 0.44$) is termed as the subthreshold region where the only attractor available is the stable focus, and the region beyond the Hopf point is the linearly unstable region ($K \geq 0.64$). The pressure-time traces in Fig. 3 correspond to the stable state and limit cycle oscillations. The frequency of observed limit cycle oscillations is 284 Hz.

For the noise-free system, the growth rate of oscillations can be estimated by fitting a straight line to the logarithmic plot of the magnitude of Hilbert transform of the acoustic pressure signal. An overview of the estimated values of growth/decay rates for a noise-free system is represented in Fig. 4 as a function of the parameter K. To determine the decay rates in the bistable region, the initially-stable system was subjected to a small perturbation to cause the oscillations to decay.

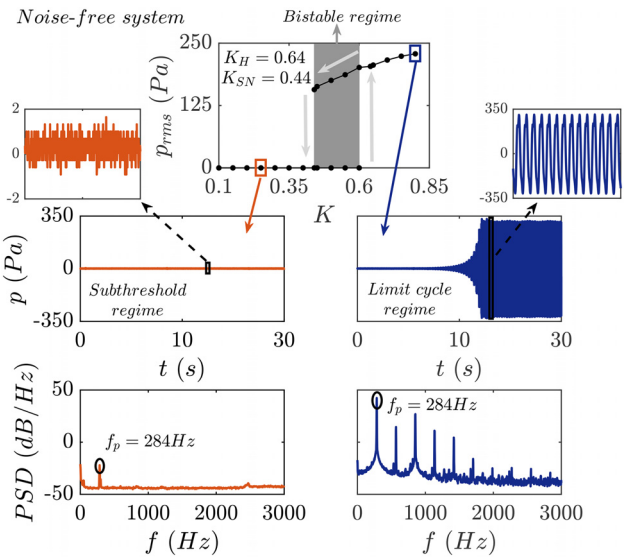

Fig. 3 Top: The subcritical Hopf bifurcation with bistable zone as the gray fill; Center: Pressure-time traces; Bottom: Power spectrum obtained for noise-free electro-acoustic Rijke tube simulator. The saddle and Hopf points are located at $K_{SN} = 0.44$ and $K_H = 0.64$, respectively. The frequency peak is at 284 Hz.

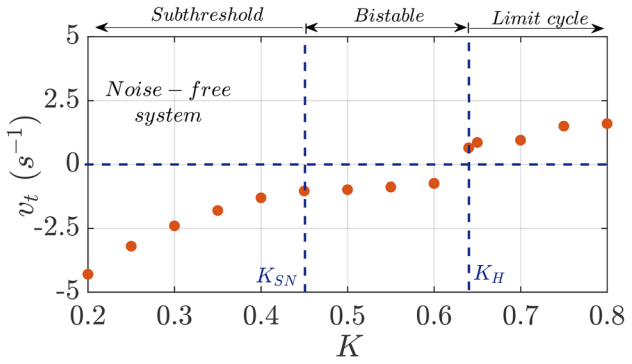

Fig. 4 An overview of the estimation of growth rates of acoustic oscillations for a noise-free system as a function of *K*

2.4 Noise-Driven Rijke Tube Simulator. Additive noise is fed into the system through LS 2 as shown in Fig. 1. We conducted two different sets of experiments for the present investigation: (i) for white-noise-driven system; (ii) for colored-noise-driven system. For white noise, we varied the noise intensity in the range of 6–23 Pa. For the colored noise experiments, the investigation is carried out for the following varying parameters:

(1) For constant variance method, we varied τ_c for different values of s^2. We varied correlation time, τ_c and the noise intensity, σ in the range of 0.1–3 ms and 7–24 Pa, respectively.
(2) For constant power in a bandwidth method, we investigated a broader range of correlation time, τ_c and noise intensity, σ varying from 0.3–35 ms and 16–54 Pa, respectively, for two bandwidths, $\Delta\omega/\omega_0 = 0.1; 0.7$ as shown in Fig. 5. In Fig. 5, the correlation time, τ_c, is normalized by the duct acoustic time period, T_0 ($= 1/f_0$).

Figure 6 shows an example of a noisy pressure-time series with the corresponding power spectrum in the subthreshold and linearly unstable regimes of the bifurcation plot for $\sigma = 17$ Pa and $\tau_c = 0.9$ ms acquired from the Rijke tube simulator.

In Sec. 3, we present the results obtained from the experimental investigation. First, we will discuss the variation of linear growth

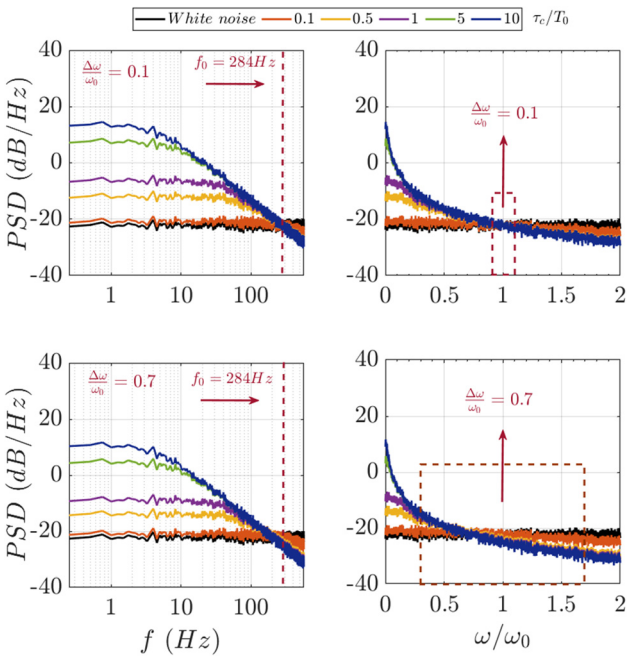

Fig. 5 Comparison between white-noise (black) and OU noise power spectra for two different bandwidths. The power provided by the two types of noise is equal in the considered band (area under the curve on linear scale).

Downloaded from http://asmedigitalcollection.asme.org/gasturbinespower/article-pdf/144/9/091017/6912725/gtp_144_09_091017.pdf by Indian Institute of Technology-Ropar user on 27 September 2022

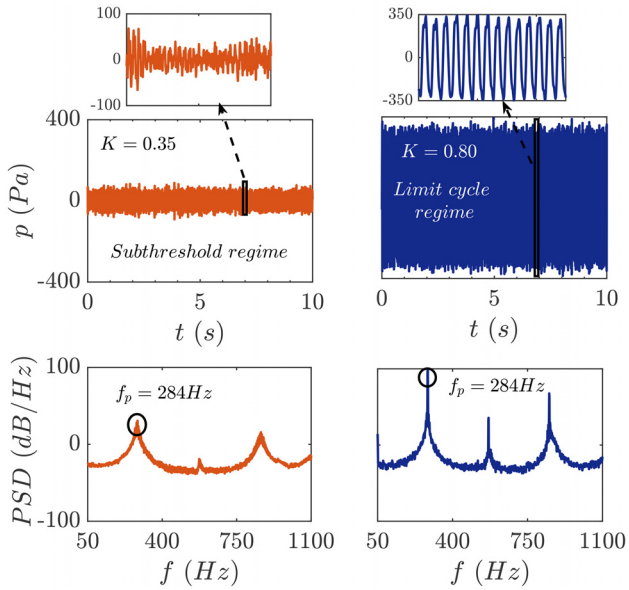

Fig. 6 An illustration of noisy pressure-time series and corresponding power spectrum in subthreshold and limit cycle regimes acquired from Rijke tube simulator for $\sigma = 17$ Pa and $\tau_c = 0.9$ ms

rates as a function of bandpass filtering and white noise amplitudes. Subsequently, we will discuss the effects of variation of colored noise parameters on growth rates. At the end, we present the comparative effects of white and colored noise (generated by the above-mentioned two methods) variation on growth rates.

3 Noise and Growth Rates Estimation

Accurate estimates of stability margins and linear growth rates of self-sustained oscillations are important for designing the damping devices for the control of thermoacoustic instabilities. The dynamics of a thermoacoustic system consists of nonlinear and stochastic effects and for accurate estimates of the growth rates, the system identification methods (SI) must take into account these aspects [24]. The SI methods developed are based on approximating the stochastic forcing as white noise (zero correlation time), however, in a real system, the stochastic forcing has a finite correlation time. In case of experimental data analysis, a theoretical "white noise PDF" given by the expression, P_w, is fitted on the experimental one, which by nature is "colored," in order to identify the growth rates. However, if the effect of noise color is not negligible in a system, the curve fit based on P_w will lead to an inaccurate parameter estimation. Here, we will investigate this deviation in the estimated growth rates when the system is subjected to white and colored noise.

3.1 Effects of White-Noise Approximations on Estimation of Growth Rates.

The concern that the noise driving a thermoacoustic system is never white in practice can bring the growth rates estimation based on white noise assumption into question. Therefore, we first estimate the growth rates using the white-noise approximation to have a comparison with the values estimated using colored noise model. By making use of the theoretical expression for $P_w(a_j)$, given by Eq. (8), to curve fit on the PDF distribution (shown in Fig. 8), we estimate the growth rates in all the three regions of the subcritical Hopf bifurcation. The term $(-\zeta_j + c_1\tau)$ in the expressions for P_c and P_w (Eqs. (7)–(8)) is the measure for growth rate estimation. We will present the overview of the estimated growth rates for the noise driven Rijke tube simulator as a two-dimensional map between noise intensity (σ) and the control parameter (K). The contours of the map will represent the relative deviation of the estimated values of the growth rates from the true values (obtained from noise-free system, given in Fig. 4).

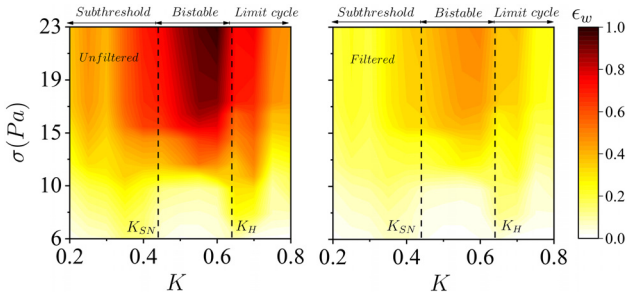

Fig. 7 Map of the deviation in estimated growth rates as a function of noise intensity (σ) and control parameter (K) considering the white noise assumption using unfiltered (left) and bandpass filtered pressure-time series (right). The contours represent the relative deviation of the estimated growth rates from the true value, given as, $\epsilon = |(v_t - v_e)|/v_t$. ϵ_w indicates the estimation of deviation for white noise.

The left plot of Fig. 7 shows the values of the estimated growth rates using the white-noise approximation on the unfiltered data for the OU noise driven simulator. As can be seen from the contours, the identified values of growth rates differ significantly from the actual values. This deviation in the values becomes more prominent (leading to a deviation of $\sim$100%) with increasing noise intensities. The reason for such deviation can be understood from the fact that the system identification methods for the growth rate estimation are derived based on the assumption of a single mode in the frequency spectrum. However, the power spectrum from the Rijke tube simulator (or real system) will consist of several excited duct acoustic modes which will be mutually coupled and will be influencing the response of each other. Therefore, we can say that the system parameter identification failed because of the lack of preprocessing of the data. To reduce the observed deviation in the estimated growth rates, we need to analyze one mode at a time. This can be easily done by bandpass filtering the data around the dominant mode. Therefore, we apply a bandpass filter around the eigenmode of the simulator ($f_0 = 284$ Hz) such that the filter discards the neighboring peaks while keeping the main peak and its tails. An example plot for applying bandpass filtering is shown in Fig. 14 in Appendix.

We then estimate the growth rates using white-noise approximation on the bandpass filtered data. The plot on the right side of

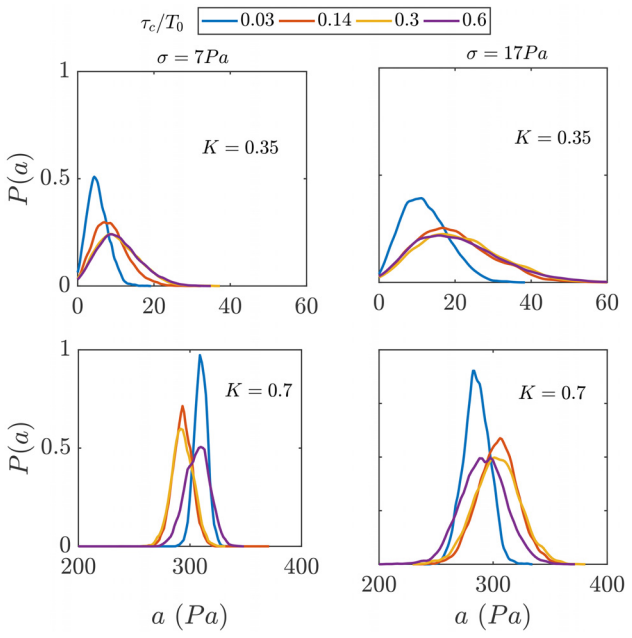

Fig. 8 PDF distribution obtained from Rijke tube simulator when driven by OU noise generated by keeping variance (s^2) constant for varied τ_c

Downloaded from http://asmedigitalcollection.asme.org/gasturbinespower/article-pdf/144/9/091017/6912725/gtp_144_09_091017.pdf by Indian Institute of Technology-Ropar user on 27 September 2022

Fig. 7 presents the estimation of growth rates. As we can observe, the deviation in the estimated values have considerably reduced by a factor of 4 in all the three regimes. In the plot, we can observe two trends: (i) in the bistable region, the deviation in the estimated growth rate values is in the range of 5–45% unlike the stable and unstable region where the observed deviation is in the range of 5–25%. This higher deviation in the estimated growth rates in bistable region is expected due to noise-induced triggering and noise-induced coherence resonance as the system approaches the saddle and Hopf points; (ii) the deviation in the estimated values increases from ∼5% to ∼45% with increasing noise intensities. This can be explained by the fact that with increasing noise intensities, the PDF becomes broader with peak values shifting toward higher values of amplitudes (also explained in Sec. 3.2 with the help of PDFs). As the noise intensity affects the distribution of PDF, therefore, the curve fit and hence growth rate estimation is also affected leading to higher deviation from the actual values.

3.2 Effects of OU Noise Generated With s^2 Constant on Estimation of Growth Rates. In this section, we now investigate the influence of colored noise parameters upon the estimation of growth rates. The Rijke tube simulator is subjected to the OU noise generated by keeping the variance constant for different combinations of τ_c and σ. Figure 8 represents the PDF distribution obtained from the bandpass filtered noisy pressure-time trace acquired from colored noise driven Rijke tube simulator for various τ_c for two different noise intensities in subthreshold and limit cycle regimes. For both subthreshold and limit cycle region, it can be seen that as the correlation time increases, the PDF becomes broader, and the peak shifts toward the higher amplitude values for both the noise power. The shift in the peak values of PDF is small at higher correlation times ($\tau_c/T_0 \geq 0.14$), and the curves overlap each other. It can also be observed that the PDF also becomes broader with increasing noise powers, leading to a decrease in the peak values. This variation of PDF distribution with τ_c and σ will affect the system identification and will lead to the deviation in the values of the estimated growth rates.

In the next step, using the theoretical expression of PDF for colored noise, $P_c(a_j)$, given by Eq. (7), we further estimate the growth rates for the eigenmode by curve fitting the expression to the experimentally obtained PDF distribution from bandpass filtered data. Figure 9 presents the overview of the estimated growth rates for the colored noise driven Rijke tube simulator. From the contours, it can be observed that the deviation in the estimated values lies within the range of 0–10% up to $\sigma = 17$Pa. When the noise intensity, $\sigma > 17$Pa, the deviation in the estimated growth rates sharply increases from 10% to ∼30%. This can be explained through the PDF distribution curves for varied noise intensities for a constant τ_c shown in Fig. 10. With increasing noise intensities, the PDF becomes broader with peak values shifting toward higher values of amplitudes. As the noise intensity affects the distribution of PDF, therefore, the curve fit and hence growth rate estimation are also affected leading to higher deviation from the actual values.

In a separate study, we also studied the noise-induced response of the Rijke tube simulator in the stable (or subthreshold) region. A characteristic feature of this subthreshold region is that noise induces unsteady fluctuations characterized by a broadband peak at the same frequency as the limit cycle oscillations that develop in the bistable region on triggering [39]. This can be observed in Fig. 6 for the Rijke tube simulator as well (noise-induced fluctuations in pressure at $K = 0.35$ are compared to the limit cycle oscillation at $K = 0.80$; the saddle node point lies at $K = 0.44$). This phenomenon is known as "coherence resonance (CR)" [40]. We observed the occurence of coherence resonance in the Rijke tube simulator and found that the noise-induced oscillations are most coherent at $\sigma_{opt} \sim 17$ Pa at $K = 0.35$ (closer to saddle point). The description and illustration of the occurence of coherence resonance phenomenon is shown in Fig. 15 in Appendix. As can be

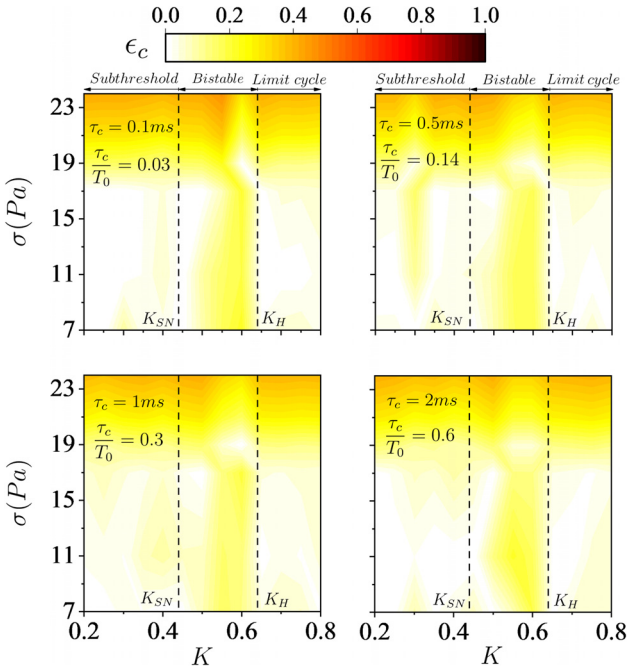

Fig. 9 Map of the deviation in estimated growth rates as a function of noise intensity (σ) and control parameter (K) from bandpass filtered data. The contours represent the relative deviation of the estimated growth rates from the true value, given as, $\epsilon = |(\nu_t - \nu_e)|/\nu_t$. ϵ_c indicates the estimation of deviation for OU noise.

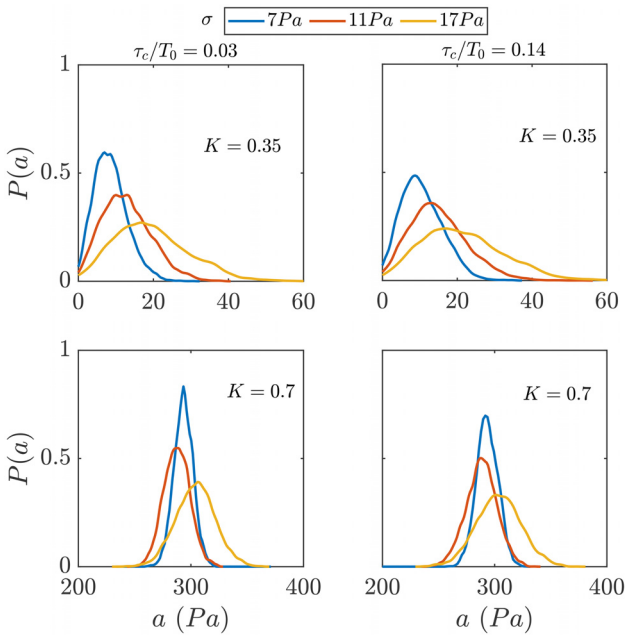

Fig. 10 PDF distribution obtained from Rijke tube simulator when driven by OU noise generated by keeping variance (s^2) constant for varied noise intensities

observed from Fig. 15, as K is varied to lower values (away from saddle point), σ_{opt} for peak coherence increases. We found that for K in the range of 0.2–0.4 and τ_c in the range of 0.1–10 ms, σ_{opt} lies within a range of 15–30 Pa. This range of σ_{opt} is closer to the values of σ above which deviation in the estimated growth rates increases by 10–20% (Fig. 9). Therefore, we can say that the noise intensities at which the deviation in estimated growth rates is high that could be related to optimum noise intensities (σ_{opt}) at which the peak coherence is induced.

Downloaded from http://asmedigitalcollection.asme.org/gasturbinespower/article-pdf/144/9/091017/6912725/gtp_144_09_091017.pdf by Indian Institute of Technology-Ropar user on 27 September 2022

Here, also, the deviation in the estimated growth rates could be more in the bistable region compared to the stable and unstable regions due to noise-induced triggering and noise-induced coherence resonance. If we compare the contours of right plot of Fig. 7 with those of Fig. 9, we can observe that the growth rate estimation is more accurate when the colored noise model is considered for a wider range of noise intensities.

Thus, it can be stated that when a system is subjected to OU noise generated by keeping variance constant, the growth rate estimation is more accurate when (i) a bandpass filter around the frequency of interest is applied; (ii) when colored noise model is used rather than white noise approximation; (iii) when the noise intensities are lower that the optimum value at which the peak coherence is induced.

In Sec. 3.3, a similar study is carried out using the second interpretation for generating the OU noise.

3.3 Effects of OU Noise Generated With Constant Power in a Bandwidth on Estimation of Growth Rates. For the investigation in this section, the Rijke tube simulator is subjected to the OU noise generated such that the powers provided by ξ and by a white noise of intensity Γ are equal in a band around the system's eigenmode. The influence of noise correlation times and the chosen bandwidths on the PDF distribution for Rijke tube simulator in subthreshold ($K = 0.35$) and limit cycle regimes ($K = 0.7$) are shown in Fig. 11. The colored noise intensity is chosen such that it has the same power within the given bandwidth as that of the white noise for all correlation times, (τ_c). In the figure, the correlation time, (τ_c), is normalized by the duct acoustic time period, (T_0), whereas the amplitude, (a), is normalized by a_m, which is the amplitude corresponding to the maximum P_w.

From the Fig. 11, significant differences in the PDF curves for white and colored noise can be observed. For subthreshold region, it can be seen that with increasing correlation times, the PDF becomes narrower, and the peak values shift toward the lower amplitudes for both the narrow and wider bandwidths when compared to the PDF of white noise. On the other hand, for the limit cycle region, the PDF becomes narrower with increasing τ_c, and the peak values shift toward the higher amplitudes for both the bandwidths. For the linearly stable region, the simulator's deterministic amplitude is 0, but the presence of noise results in a nonzero amplitude of maximum probability. Whereas, for the linearly unstable case, the amplitude of maximum probability for the colored noise does not change. Therefore, it can be stated that for both the regions, subthreshold and limit cycle regions, the colored noise let the system stay closer to its deterministic amplitude when compared to the white noise of same power. This trend can be attributed to the noise correlation time. The differences in the PDFs of white and colored noise can affect the growth rate estimation. We now estimate the values of growth rates by curve fitting the PDF expression, P_c, on the experimental PDFs as a function of τ_c and σ.

Figure 12 presents the overview of the estimated growth rates for $\Delta\omega/\omega_0 = 0.7$ in all the three regions of the subcritical Hopf bifurcation. From the contours, we can observe that the deviation in the estimated growth rates increases from 5% to ~60% with increasing noise intensities independent of τ_c. In this case, the optimum value of noise intensity above which the deviation is sharply increased is found to be $\sigma_{opt} = 33$Pa. Also, the deviation is higher in bistable region due to noise-induced triggering and noise-induced coherence resonance. For noise levels below 16 Pa, the estimated growth rates are closer to the true values and to those predicted by the white-noise approximation.

3.4 Effect of OU Process Correlation Time on Estimation of Growth Rates. In this section, we investigate the influence of correlation times of the driving OU noise upon growth rate estimation for both the interpretations of the noise generation. The deviation of the estimated growth rates from the true values are presented in form of a two-dimensional map between τ_c and control parameter, K and is shown in Fig. 13. It can be observed from the contours that the deviation in the estimated growth rate values is in the range of 0–15% when the colored noise model is used for system identification compared to white-noise approximation,

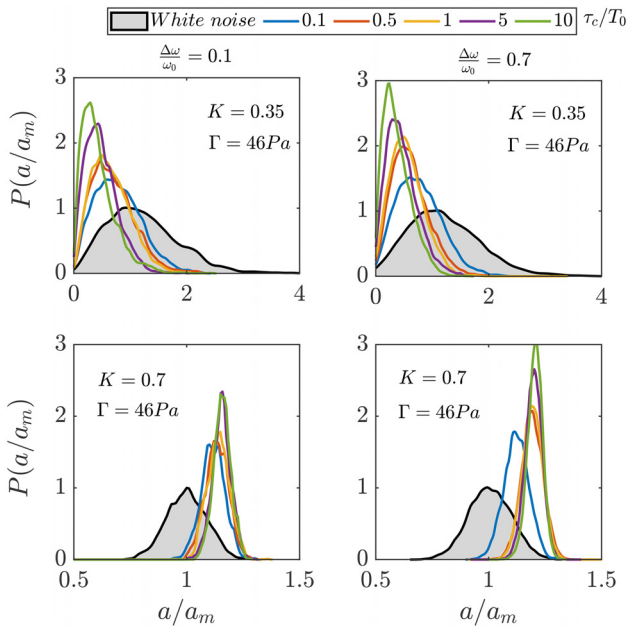

Fig. 11 PDF distribution obtained from Rijke tube simulator when driven by OU noise generated by keeping power in a bandwidth constant for two bandwidths and five correlation times in subthreshold and limit cycle regions. τ_c is normalized by acoustic time period, T_0 whereas, amplitude, a, is normalized by a_m which is the amplitude corresponding to maximum P_w.

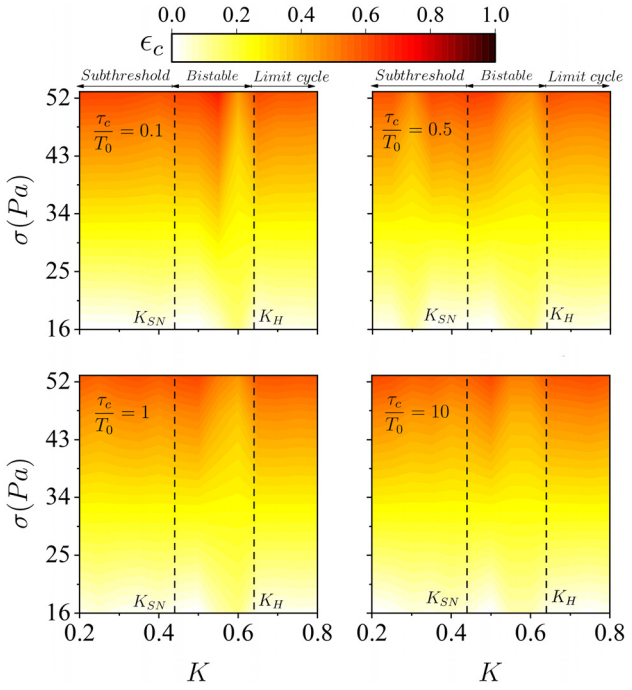

Fig. 12 Map of the deviation in estimated growth rates as a function of noise intensity (σ) and control parameter (K) for $\Delta\omega/\omega_0 = 0.7$ and varied τ_c. The contours represent the relative deviation of the estimated growth rates from the true value, given as, $\epsilon = |(v_t - v_e)|/v_t$. ϵ_c indicates the estimation of deviation for OU noise.

Downloaded from http://asmedigitalcollection.asme.org/gasturbinespower/article-pdf/144/9/091017/6912725/gtp_144_09_091017.pdf by Indian Institute of Technology-Ropar user on 27 September 2022

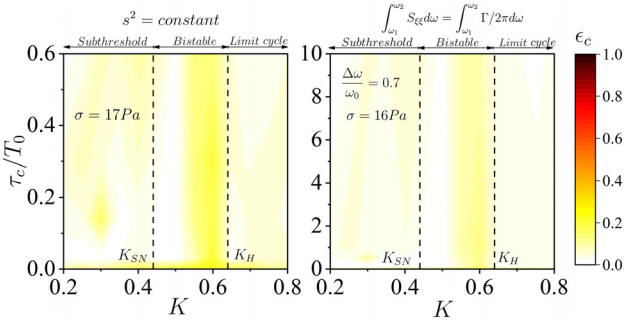

Fig. 13 Map of the deviation in estimated growth rates as a function of correlation time (τ_c) and control parameter (K) for both the interpretations of colored noise generation and white noise. The contours represent the relative deviation of the estimated growth rates from the true value, given as, $\epsilon = |(v_t - v_e)|/v_t$. $\tau_c = 0$ represents the white noise case. ϵ_c indicates the estimation of deviation for OU noise.

where the deviation lies within the range of 10–20%, when the noise is generated keeping variance constant. However, when the noise is generated by keeping power in a bandwidth constant, the results are closer to those predicted by the white-noise approximation (deviation is within 0–10%). The deviation, however, is higher in the bistable region than in the subthreshold and limit cycle regions. This could be because of the noise-induced triggering and noise-induced coherence resonance, which affects the growth rate estimate, as the system approaches the saddle point as shown in Fig. 15.

Summarizing, in case of the real systems, we acquire noisy pressure-time trace with no prior knowledge of the noise intensity or noise correlation time to which the system is subjected. In our study, we investigated the influence of two types of noise models: colored and white noise on growth rates estimation. We found that for a robust parameter identification, the following criteria must be taken into account: (i) preprocessing of the noisy data (applying bandpass filtering around the peak frequency); (ii) the regions of the Hopf bifurcation in which the estimation is done; (iii) using the colored noise model rather than white noise approximation for estimation; (iv) the influence of noise amplitudes on the estimated growth rates.

4 Conclusions

In this work, we report the influence of OU type colored noise on thermoacoustic coupling using an electro-acoustic Rijke tube simulator. We considered two different interpretations for generating OU type colored noise: (i) by keeping variance, s^2, constant and varying τ_c; (ii) by keeping the powers provided by OU noise (ξ) and by a white noise of intensity Γ in a band around the system's natural frequency equal. We investigated the effects of noise intensity and correlation time on the estimation of growth rates of oscillations (determined using Fokker–Planck equation) in the stable, bistable and linearly unstable regions. Subsequently, we compare the findings against results obtained using white noise approximations. From our investigation, we draw the following significant conclusions:

(1) Increasing the correlation time (τ_c) and noise intensity (σ) leads to an increase in the deviation of the estimated growth rates from the true values. For $\sigma < \sigma_{\text{opt}}$, the deviation in the estimated values lies within the range of 0–10% but when $\sigma > \sigma_{\text{opt}}$, the deviation increases from 10% to 30%. A sharp increase in the deviation of the estimated growth rates above σ_{opt} can be attributed to the fact that higher noise intensities affects the non-linear and stochastic dynamics of the system thus affecting the system identification.
(2) This optimum value of noise intensity above which the deviation in the estimated growth rates sharply increases is close to the value at which the peak coherence is induced in the system.
(3) For colored noise model, the deviation in the estimated growth rates lies within the range of 0–10% compared to the deviation of 5–25% observed considering the white noise approximation.
(4) The accuracy in the estimated growth rates can be increased by (i) applying a bandpass filter around the frequency of interest; (ii) using the Fokker–Planck equation based on colored noise model for growth rate estimation rather than white noise model; (iii) when the noise intensities are lower that the optimum value at which the peak coherence is induced.
(5) The effect of noise-induced triggering in the bistable zone manifested in the form of a higher deviation of the estimated growth rates from the actual values.

In terms of practical implications of the study, the result that higher noise intensity leads to inaccurate system identification is crucial to designing acoustic damping devices for the control of thermoacoustic instabilities. In particular, the deviations observed in the estimated growth rate (or the decay rate) will lead to failure of decay-rate-based early warning indicators of thermoacoustic instabilities.

Acknowledgment

The financial support received from MHRD and the institute seed funding for conducting the research on the topic of stochastically forced thermoacoustic system and instabilities is highly appreciated. VG is supported by the National Natural Science Foundation of China (Grant Nos. 12002147 and 12050410247).

Funding data

- MHRD and the Institute Seed Funding (IIT Ropar) (No. 9-277/2017/IITRPR/4854; Funder ID: 10.13039/501100018978).
- National Natural Science Foundation of China (Grant Nos. 12002147 and 12050410247; Funder ID: 10.13039/501100001809).

Nomenclature

a_j = amplitude of jth mode
A = amplitude of oscillations
c_0 = speed of sound
c_p = specific heat at constant pressure
c_v = specific heat at constant volume
c_1, c_2, c_3 = constants
C = normalizing constant
C_1, C_2 = damping coefficients
D = colored noise intensity
f = frequency
$g(\eta)$ = function of η
K = normalized heater power
K_H = Hopf point
K_{SN} = saddle point
L_a = length of Rijke tube
Ma = Mach number
N = number of acoustic modes
OU = Ornstein–Uhlenbeck process
p = normalized acoustic pressure
$P_c(a_j)$ = PDF of OU process
$P_w(a_j)$ = PDF of white noise
PDF = probability distribution function
PSD = power spectral density
$\dot{Q}'$ = heat release rate fluctuations

Downloaded from http://asmedigitalcollection.asme.org/gasturbinespower/article-pdf/144/9/091017/6912725/gtp_144_09_091017.pdf by Indian Institute of Technology-Ropar user on 27 September 2022

s^2 = variance of OU process
$S_{\epsilon\epsilon}(\omega)$ = power spectral density of white noise
$S_{\xi\xi}(\omega)$ = power spectral density of OU noise
SDE = stochastic differential equation
t = Normalized time
T_0 = acoustic time period
u = normalized acoustic velocity
u_f = acoustic velocity at x_f
v_e = estimated values of growth rates
v_t = true values of growth rates
x = normalized axial direction
x_f = axial location of heater wire mesh
α = cold decay rates of acoustic oscillations
γ = ratio of specific heats at constant pressure and volume
δ = Dirac delta function
ϵ = deviation of growth rates from true values
$\epsilon(t)$ = Gaussian white noise
ζ_j = acoustic damping
η = modal amplitude
$\xi(t)$ = OU type colored noise
ρ = density of air
σ = RMS of noise intensity
τ = time delay
τ_c = noise correlation time
ω_0 = eigenfrequency
Γ = white noise intensity
$\phi(t)$ = phase
$()_0$ = mean quantity

Appendix

Fokker–Planck Equation for Closed–Closed Rijke Tube. On substituting the Galerkin's decomposition in acoustic momentum and energy equations (Eq. (1)), adding the additive noise term and combining the two subequations of Eq. (4), for any jth mode, we obtain

$$\frac{d\dot{\eta}_j}{dt}+\zeta_j\dot{\eta}_j+(j\pi)^2\eta_j = \frac{K(j\pi)\cos(j\pi x_f)}{\sqrt{3}}\left[\sqrt{\left|1+3\sin(j\pi x_f)\eta_j(t-\tau)\right|}-1\right]+\xi_j \tag{A1}$$

For weakly nonlinear analysis of the reduced-order Rijke tube model given by Eq. (A1), we assume small magnitudes of η and expand the square-root nonlinearity in a Maclaurin series to obtain

$$\frac{d\dot{\eta}_j}{dt}+\zeta_j\dot{\eta}_j+(j\pi)^2\eta_j = \frac{\sqrt{3}}{4}K(j\pi)\sin(2j\pi x_f)\left[\eta(t-\tau)-\frac{3}{4}\sin(j\pi x_f)\eta(t-\tau)^2+\frac{9}{8}\sin^2(j\pi x_f)\eta(t-\tau)^3\right]+\xi_j \tag{A2}$$

Now, in order to simplify, we introduce the following terms in Eq. (A2)

$$c_1=\frac{\sqrt{3}Kj\pi}{4}\sin(2j\pi x_f);\quad c_2=-\frac{3\sqrt{3}Kj\pi}{16}\sin(2j\pi x_f)\sin(j\pi x_f);$$
$$c_3=\frac{9\sqrt{3}Kj\pi}{32}\sin(2j\pi x_f)\sin^2(j\pi x_f)$$

and obtain

$$\frac{d\dot{\eta}_j}{dt}+\zeta_j\dot{\eta}_j+(j\pi)^2\eta_j+c_1\eta(t-\tau)+c_2\eta(t-\tau)^2+c_3\eta(t-\tau)^3-\xi_j=0 \tag{A3}$$

Now, for small τ, $\eta(t-\tau)$ can be approximated as

$$\begin{aligned}\eta(t-\tau)&\approx\eta(t)-\tau\dot{\eta}(t)\\ \eta(t-\tau)^2&\approx\eta^2(t)+\tau^2\dot{\eta}^2(t)-2\tau\eta(t)\dot{\eta}(t)\\ \eta(t-\tau)^3&\approx\eta^3(t)-\tau^3\dot{\eta}^3(t)-3\tau\eta^2(t)\dot{\eta}(t)+3\tau^2\eta(t)\dot{\eta}^2(t)\end{aligned} \tag{A4}$$

Now, combining Eqs. (A3) and (A4), we obtain the following linearized equation for jth mode

$$\frac{d\dot{\eta}_j}{dt}+\zeta_j\dot{\eta}_j+(j\pi)^2\eta_j+c_1\eta_j-c_1\tau\dot{\eta}_j+c_2\eta^2+c_2\tau^2\dot{\eta}_j^2-2c_2\tau\eta_j\dot{\eta}_j+c_3\eta_j^3-c_3\tau^3\dot{\eta}_j^3-3c_3\tau\eta_j^2\dot{\eta}_j+3c_3\tau^2\eta_j\dot{\eta}_j^2-\xi_j=0 \tag{A5}$$

Now, we derive the Fokker–Planck equation representing the probability density function (PDF) of the amplitude of the pressure fluctuations inside the Rijke tube. To obtain an explicit form of the stationary Fokker–Planck equation, we derive the Fokker–Planck equation for the jth mode.

The state variable, η_j and $\dot{\eta}_j$ can be transformed into amplitude and phase equations using the following relation:

$$\begin{aligned}\eta_j&=a_j\cos(\omega_j t+\varphi_j)\\ \dot{\eta}_j&=-a_j\omega_j\sin(\omega_j t+\varphi_j)\end{aligned} \tag{A6}$$

where a_j and φ_j are the instantaneous amplitude and phase of η_j. We transform Eq. (A5) in terms of a_j and φ_j as

$$\begin{aligned}&\dot{a}_j\cos\phi_j-a_j\dot{\varphi}_j\sin\phi_j=0\\ &\dot{a}_j\sin\phi_j+a_j\dot{\varphi}_j\cos\phi_j=-\zeta_j a_j\sin\phi_j+c_1\tau a_j\sin\phi_j\\ &\quad+\frac{c_1}{\omega_j}a_j\cos\phi_j+\frac{c_2}{\omega_j}a_j^2\cos^2\phi_j+2c_2\tau a_j^2\sin\phi_j\cos\phi_j\\ &\quad+c_2\tau^2a_j^2\omega_j\sin^2\phi_j+\frac{c_3}{\omega_j}a_j^3\cos^3\phi_j+3c_3\tau a_j^3\sin\phi_j\cos^2\phi_j\\ &\quad+3c_3\tau^2a_j{}^3\omega_j\sin^2\phi_j\cos\phi_j\\ &\quad+c_3\tau^3a_j^3\omega_j^2\sin^3\phi_j+\xi_j\end{aligned} \tag{A7}$$

where $\phi_j=\omega_j t+\varphi_j$. The ordinary differential equations for a_j and φ_j obtained from Eq. (A7) are as

$$\begin{aligned}\dot{a}_j&=-\frac{\zeta_j a_j}{2}+\frac{c_1\tau a_j}{2}+\frac{3c_3\tau^3a_j^3\omega_j^2}{8}+\frac{3c_3\tau a_j^3}{8}+Q_a(a,\phi)+\frac{\xi_j}{\omega_j}(\sin\phi)\\ \dot{\varphi}_j&=\frac{c_1}{2\omega_j}+\frac{3c_3a_j^2}{8\omega_j}+\frac{3c_3\tau^2a_j^2\omega_j}{8}+Q_\phi(a,\phi)+\frac{\xi_j}{a_j\omega_j}(\cos\phi)\end{aligned} \tag{A8}$$

where, $Q_a(a,\phi)$ and $Q_\phi(a,\phi)$ are the sum of first-order sine and cosine terms that become zero after time-averaging. To derive the stochastic equations for a_j and φ_j, following the method stated in Ref. [37], we perform averaging of Eq. (A8) over one cycle of oscillation. The stochastic part of Eq. (A8) can be transformed using, $x=\xi(t)\sin\phi(t)$ and $y=\xi(t)\cos\phi(t)$. The correlation time of noise is assumed to be much smaller than the characteristic time of a_j, hence there exists a time shift $\Delta\gg\tau_c$, over which a_j and φ do not change noticeably. We can then expand x in φ, around $\varphi(t-\Delta)=\varphi_{-\Delta}$ as

$$x\approx-\xi(t)\sin(\omega_j t+\varphi_{-\Delta})-\xi(t)\cos(\omega_j t+\varphi_{-\Delta})\Delta\varphi$$

Downloaded from http://asmedigitalcollection.asme.org/gasturbinespower/article-pdf/144/9/091017/6912725/gtp_144_09_091017.pdf by Indian Institute of Technology-Ropar user on 27 September 2022

We can then integrate the fluctuating term of Eq. (A8), obtain $\Delta\varphi$, and then express $\langle x\rangle$ as

$$\langle x\rangle = -\frac{1}{\omega_j a_j}\int_0^{\Delta}\langle\xi\xi_{\tau-0}\rangle\cos\phi\cos\left(\phi-\omega_j\tau_0\right)d\tau$$

For OU noise, $\langle\xi\xi_{\tau_0}\rangle = \Gamma\frac{\gamma}{2\tau_c}e^{-\tau_0/\tau_c}$. This autocorrelation function tends to zero for time larger than τ_c. Therefore, we get

$$\langle x\rangle/\omega_j = \dot{a}_{j\,\text{stoch}} = \frac{\Gamma}{4\omega_j^2 a_j}\frac{\sqrt{D}}{\left(1+\omega_j^2\tau_c^2\right)} \tag{A9}$$

This term exists due to the correlation between $a_j(t)$ and $\varphi(t)$, which causes the fluctuating component to have a nonzero average.

For white noise, $\tau_c \to 0$ and $D \to 1$, hence, we get

$$\langle x\rangle/\omega_j = \dot{a}_{j\,\text{stoch}} = \frac{\Gamma}{4\omega_j^2 a_j} \tag{A10}$$

Making use of Eqs. (A8)–(A10), we compute the following form of Fokker–Planck equation

$$\frac{\partial}{\partial t}P(a_j,t) = -\frac{\partial}{\partial a_j}\left[m(a_j)P(a_j,t)\right] + \frac{\partial^2}{\partial a_j^2}\left[\frac{\sigma(a_j)}{2}P(a_j,t)\right] \tag{A11}$$

where the drift and diffusion coefficients are given as

$$\begin{aligned} m(a_j) &= -\frac{\zeta_j a_j}{2} + \frac{c_1\tau a_j}{2} + \frac{3c_3\tau a_j^3}{8} + \frac{3c_3\tau^3\omega_j^2 a_j^3}{8} + \frac{\Gamma}{4\omega_j^2 a_j} \\ \sigma(a_j) &= \frac{\Gamma}{2\omega_j^2} \end{aligned} \tag{A12}$$

Integration of Eq. (A11) will yield the following stationary PDF for OU noise

$$\begin{aligned} P_c(a_j) = C_c a_j \exp\Bigg[&\left(-\zeta_j + c_1\tau\right)\frac{4\omega_j^2 a_j^2}{\Gamma}\frac{\left(1+\omega_j^2\tau_c^2\right)}{\sqrt{D}} \\ &+\left(1+\omega_j^2\tau^2\right)\frac{12c_3\tau a_j^4\omega_j^2}{8\Gamma}\frac{\left(1+\omega_j^2\tau_c^2\right)}{\sqrt{D}}\Bigg] \end{aligned} \tag{A13}$$

and for the white noise as

$$P_w(a_j) = C_w a_j \exp\left[\left(-\zeta_j + c_1\tau\right)\frac{4\omega_j^2 a_j^2}{\Gamma} + \left(1+\omega_j^2\tau^2\right)\frac{12c_3\tau a_j^4\omega_j^2}{8\Gamma}\right] \tag{A14}$$

where C_c and C_w are the normalization constants such that $\int_0^\infty P(a_j)da_j = 1$.

Bandpass Filtering of Noisy Pressure-Time Trace. An illustration of bandpass filtering applied to the noisy pressure-time series acquired from Rijke tube simulator is presented in Fig. 14. The Rijke tube simulator is subjected to OU type noise generated keeping the variance constant. The bandpass filtering is applied around the eigenfrequency such that the filter discards the neighboring peaks while keeping the main peak and its tails.

Coherence Resonance. The phenomenon of coherence resonance is a result of a nonlinear interaction between noise and the acoustic mode of the system that becomes unstable after the Hopf bifurcation [39]. Coherent oscillations that are induced by noise in the subthreshold region are dependent on the noise intensity: the induced coherence attains a peak at an intermediate noise intensity and on the proximity of the system to the Hopf bifurcation such that, the optimum intensity shifts to lower values as the system is brought closer to the Hopf bifurcation and the induced coherence increases [20]. The induced coherence is quantified in the form of a coherence factor, β [41,42] defined as, $\beta = H_p \times \left(\frac{\Delta f}{f_p}\right)^{-1}$, where H_p and $\Delta f/f_p$ are the height and normalized width (normalized by the peak frequency) of a Lorentzian fit to the broadband spectral peak; the width is measured at half the height of the peak of the fit.

We also investigated the effect of colored noise intensity (σ) variation on the coherence factor for a given value of τ_c. Figure 15 presents the variation of β with respect to σ for fixed τ_c. The hallmark of coherence resonance—the resonance-like variation of coherence factor with respect to noise intensity—is clear in the plots. Furthermore, we also see that as the value of K is increased toward the saddle point ($K = 0.44$), the induced coherence is higher, and the peak coherence (indicated by dashed vertical lines) is induced at smaller values of noise intensity, σ (shown by the arrows). From Fig. 15, it can be observed that for $K = 0.35$ and $\tau_c = 0.1$ms, the peak coherence is induced at $\sigma_{\text{opt}} \sim 17$Pa. This indicates that the self-induced oscillations are most coherent at this σ_{opt}. We found that for K in the range of 0.2–0.4 and τ_c in the range of 0.1–10 ms, σ_{opt} lies within a range of 15–30 Pa. This range of σ_{opt} is closer to the values of σ above which deviation in

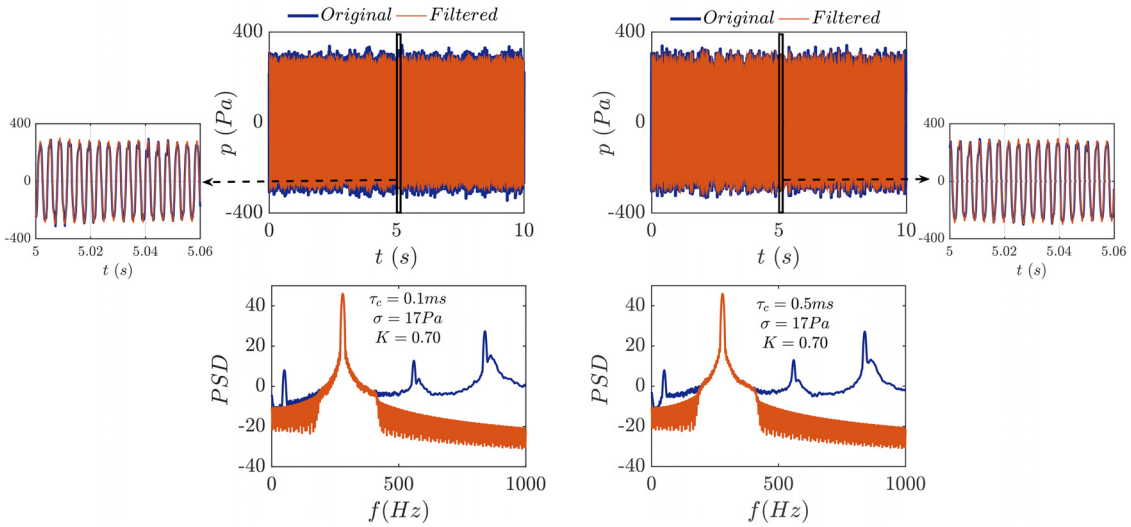

Fig. 14 An illustration of bandpass filtering of pressure-time series and its corresponding power spectrum obtained from colored noise driven Rijke tube simulator

Downloaded from http://asmedigitalcollection.asme.org/gasturbinespower/article-pdf/144/9/091017/6912725/gtp_144_09_091017.pdf by Indian Institute of Technology-Ropar user on 27 September 2022

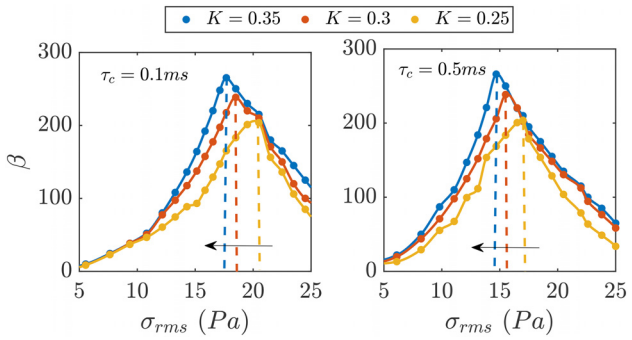

Fig. 15 Variation of coherence factor, β, as a function of noise intensity, σ, for fixed values of τ_c. β attains maxima for an optimum value of σ indicating the presence of coherence resonance. As K is brought closer to the saddle point, the optimum value of σ shifts toward lower values.

the estimated growth rates increases by 10–20% (Fig. 9). Therefore, we can say that the noise intensities at which the deviation in estimated growth rates is high could be related to optimum noise intensities (σ_{opt}) at which the peak coherence is induced.

References

[1] Lieuwen, T. C., and Yang, V., 2005, *Combustion Instabilities in Gas Turbine Engines: Operational Experience, Fundamental Mechanisms, and Modeling*, American Institute of Aeronautics and Astronautics, Reston, VA.

[2] Bernhard, R. J., Hall, H. R., and Jones, J. D., 1992, "Adaptive-Passive Noise Control," *Internoise*, Vol. 139, pp. 427–427, Noise Control Foundation.

[3] Noiray, N., and Schuermans, B., 2012, "Theoretical and Experimental Investigations on Damper Performance for Suppression of Thermoacoustic Oscillations," J. Sound Vib., **331**(12), pp. 2753–2763.

[4] Lieuwen, T. C., 2002, "Experimental Investigation of Limit-Cycle Oscillations in an Unstable Gas Turbine Combustor," J. Propul. Power, **18**(1), pp. 61–67.

[5] Kabiraj, L., and Sujith, R. I., 2011, "Investigation of Subcritical Instability in Ducted Premixed Flames," ASME Paper No. GT2011-46155.

[6] Kabiraj, L., Saurabh, A., Wahi, P., and Sujith, R., 2012, "Route to Chaos for Combustion Instability in Ducted Laminar Premixed Flames," Chaos, **22**(2), p. 023129.

[7] Kabiraj, L., Saurabh, A., Karimi, N., Sailor, A., Mastorakos, E., Dowling, A. P., and Paschereit, C. O., 2015, "Chaos in an Imperfectly Premixed Model Combustor," Chaos, **25**(2), p. 023101.

[8] Juniper, M. P., 2011, "Triggering in the Horizontal Rijke Tube: Non-Normality, Transient Growth and Bypass Transition," J. Fluid Mech., **667**, pp. 272–308.

[9] Waugh, I. C., and Juniper, M. P., 2011, "Triggering in a Thermoacoustic System With Stochastic Noise," Int. J. Spray Combust. Dyn., **3**(3), pp. 225–241.

[10] Jegadeesan, V., and Sujith, R., 2013, "Experimental Investigation of Noise Induced Triggering in Thermoacoustic Systems," Proc. Combust. Inst., **34**(2), pp. 3175–3183.

[11] Lieuwen, T., and Banaszuk, A., 2005, "Background Noise Effects on Combustor Stability," J. Propul. Power, **21**(1), pp. 25–31.

[12] Gopalakrishnan, E., and Sujith, R., 2015, "Effect of External Noise on the Hysteresis Characteristics of a Thermoacoustic System," J. Fluid Mech., **776**, pp. 334–353.

[13] Noiray, N., and Schuermans, B., 2013, "Deterministic Quantities Characterizing Noise Driven Hopf Bifurcations in Gas Turbine Combustors," Int. J. Non-Linear Mech., **50**, pp. 152–163.

[14] Noiray, N., 2017, "Linear Growth Rate Estimation From Dynamics and Statistics of Acoustic Signal Envelope in Turbulent Combustors," ASME J. Eng. Gas Turbines Power, **139**(4), p. 041503.

[15] Boujo, E., and Noiray, N., 2017, "Robust Identification of Harmonic Oscillator Parameters Using the Adjoint Fokker–Planck Equation," Proc. R. Soc. A, **473**(2200), p. 20160894.

[16] Noiray, N., and Denisov, A., 2017, "A Method to Identify Thermoacoustic Growth Rates in Combustion Chambers From Dynamic Pressure Time Series," Proc. Combust. Inst., **36**(3), pp. 3843–3850.

[17] Seywert, C. N., 2001, "Combustion Instabilities: Issues in Modeling and Control," Ph.D. thesis, California Institute of Technology, Pasedena, CA.

[18] Burnley, V. S., 1996, "Nonlinear Combustion Instabilities and Stochastic Sources," Ph.D. thesis, California Institute of Technology, Pasedena, CA.

[19] Vishnoi, N., Wahi, P., Saurabh, A., and Kabiraj, L., 2021, "On the Effect of Noise Induced Dynamics on Linear Growth Rates of Oscillations in an Electro-acoustic Rijke Tube Simulator," ASME Paper No. GT2021-58691.

[20] Kabiraj, L., Steinert, R., Saurabh, A., and Paschereit, C. O., 2015, "Coherence Resonance in a Thermoacoustic System," Phys. Rev. E, **92**(4), p. 042909.

[21] Saurabh, A., Kabiraj, L., Steinert, R., and Oliver Paschereit, C., 2017, "Noise-Induced Dynamics in the Subthreshold Region in Thermoacoustic Systems," ASME J. Eng. Gas Turbines Power, **139**(3), p, 031508.

[22] Lee, M., Zhu, Y., Li, L. K., and Gupta, V., 2019, "System Identification of a Low-Density Jet Via Its Noise-Induced Dynamics," J. Fluid Mech., **862**, pp. 200–215.

[23] Rajaram, R., and Lieuwen, T., 2009, "Acoustic Radiation From Turbulent Premixed Flames," J. Fluid Mech., **637**, pp. 357–385.

[24] Bonciolini, G., Boujo, E., and Noiray, N., 2016, "Effects of Turbulence-Induced Colored Noise on Thermoacoustic Instabilities in Combustion Chambers," International Symposium: Thermoacoustic Instabilities in Gas Turbines and Rocket Engines, ETH Zürich, Munich, Germany, May 30–June 2.

[25] Bonciolini, G., Boujo, E., and Noiray, N., 2017, "Output-Only Parameter Identification of a Colored-Noise-Driven Van-Der-Pol Oscillator: Thermoacoustic Instabilities as an Example," Phys. Rev. E, **95**(6), p. 062217.

[26] Li, X., Wang, Y., Wang, N., and Zhao, D., 2020, "Stochastic Properties of Thermoacoustic Oscillations in an Annular Gas Turbine Combustion Chamber Driven by Colored Noise," J. Sound Vib., **480**, p. 115423.

[27] Feldman, K. T., Jr, 1968, "Review of the Literature on Rijke Thermoacoustic Phenomena," J. Sound Vib., **7**(1), pp. 83–89.

[28] Heckl, M. A., 1990, "Non-Linear Acoustic Effects in the Rijke Tube," Acta Acust., **72**(1), pp. 63–71.

[29] Raun, R., Beckstead, M., Finlinson, J., and Brooks, K., 1993, "A Review of Rijke Tubes, Rijke Burners and Related Devices," Prog. Energy Combust. Sci., **19**(4), pp. 313–364.

[30] Nicoud, F., and Wieczorek, K., 2009, "About the Zero Mach Number Assumption in the Calculation of Thermoacoustic Instabilities," Int. J. Spray Combust. Dyn., **1**(1), pp. 67–111.

[31] Gupta, V., Saurabh, A., Paschereit, C. O., and Kabiraj, L., 2017, "Numerical Results on Noise-Induced Dynamics in the Subthreshold Regime for Thermoacoustic Systems," J. Sound Vib., **390**, pp. 55–66.

[32] Matveev, K. I., and Culick, F., 2003, "A Model for Combustion Instability Involving Vortex Shedding," Combust. Sci. Technol., **175**(6), pp. 1059–1083.

[33] Sterling, J., and Zukoski, E., 1991, "Nonlinear Dynamics of Laboratory Combustor Pressure Oscillations," Combust. Sci. Technol., **77**(4–6), pp. 225–238.

[34] Ma, J., Xiao, T., Hou, Z., and Xin, H., 2008, "Coherence Resonance Induced by Colored Noise Near Hopf Bifurcation," Chaos, **18**(4), p. 043116.

[35] Miguel, M. S., and Toral, R., 2000, "Stochastic Effects in Physical Systems," *In Instabilities and Nonequilibrium Structures VI*, Springer, Dordrecht, The Netherlands, pp. 35–127.

[36] Beato, V., Sendina-Nadal, I., Gerdes, I., and Engel, H., 2008, "Coherence Resonance in a Chemical Excitable System Driven by Coloured Noise," Philos. Trans. R. Soc., A **366**(1864), pp. 381–395.

[37] Stratonovich, R. L., 1967, *Topics in the Theory of Random Noise*, Vol. 2, CRC Press, Boca Raton, FL.

[38] Gardiner, C. W, et al., 1985, *Handbook of Stochastic Methods*, Vol. 3, Springer, Berlin.

[39] Wiesenfeld, K., 1985, "Noisy Precursors of Nonlinear Instabilities," J. Stat. Phys., **38**(5–6), pp. 1071–1097.

[40] Pikovsky, A. S., and Kurths, J., 1997, "Coherence Resonance in a Noise-Driven Excitable System," Phys. Rev. Lett., **78**(5), pp. 775–778.

[41] Neiman, A., Saparin, P. I., and Stone, L., 1997, "Coherence Resonance at Noisy Precursors of Bifurcations in Nonlinear Dynamical Systems," Phys. Rev. E, **56**(1), pp. 270–273.

[42] Ushakov, O., Wünsche, H.-J., Henneberger, F., Khovanov, I., Schimansky-Geier, L., and Zaks, M., 2005, "Coherence Resonance Near a Hopf Bifurcation," Phys. Rev. Lett., **95**(12), p. 123903.

Downloaded from http://asmedigitalcollection.asme.org/gasturbinespower/article-pdf/144/9/091017/6912725/gtp_144_09_091017.pdf by Indian Institute of Technology-Ropar user on 27 September 2022